

# *Sustainable electrospinning of nanoscale fibres*

Article

Published Version

Creative Commons: Attribution-Noncommercial-No Derivative Works 4.0

Open access

Alazab, M., Mitchell, G. R., Davis, F. J. ORCID:  
<https://orcid.org/0000-0003-0462-872X> and Mohan, S. D.  
(2017) Sustainable electrospinning of nanoscale fibres.  
Procedia Manufacturing, 12. pp. 66-78. ISSN 2351-9789 doi:  
<https://doi.org/10.1016/j.promfg.2017.08.009> Available at  
<https://centaur.reading.ac.uk/73423/>

It is advisable to refer to the publisher's version if you intend to cite from the work. See [Guidance on citing](#).

Published version at: <https://www.sciencedirect.com/science/article/pii/S235197891730598X>

To link to this article DOI: <http://dx.doi.org/10.1016/j.promfg.2017.08.009>

Publisher: Elsevier

All outputs in CentAUR are protected by Intellectual Property Rights law, including copyright law. Copyright and IPR is retained by the creators or other copyright holders. Terms and conditions for use of this material are defined in the [End User Agreement](#).

[www.reading.ac.uk/centaur](http://www.reading.ac.uk/centaur)

**CentAUR**

Central Archive at the University of Reading

Reading's research outputs online





International Conference on Sustainable and Intelligent Manufacturing, RESIM 2016, 14-17  
December 2016, Leiria, Portugal

## Sustainable electrospinning of nanoscale fibres

Mohamed Alazab<sup>a</sup>, Geoffrey R. Mitchell<sup>b,c\*</sup>, Fred J. Davis<sup>d</sup> and Saeed D. Mohan<sup>d</sup>

<sup>a</sup>Department of Chemistry, College of Science, United Arab Emirates University, Alain City, UAE

<sup>b</sup>Centre for Rapid and Sustainable Product Development, Institute Polytechnic of Leiria, Rua de Portugal, Marinha Grande, 2430-028, Portugal

<sup>c</sup>Centre for Advanced Microscopy, University of Reading, Whiteknights, Reading, RG6 6AF UK

<sup>d</sup>Department of Chemistry, University of Reading, Whiteknights, RG6 6AD, UK

### Abstract

Electrospinning is an effective technology for the preparation of nano and micro scale fibres for diverse application in oil recovery, medical devices, and filters. It is achieved by injecting a charged solution of polymeric material through a needle into a region of high electric field. Under these conditions, the expelled jet follows a chaotic, whip-like trajectory towards a grounded collection plate. At low polymer concentrations, the high forces experienced by the jet prior to becoming grounded on the collection plate, result in the formation of undesirable discrete droplets of material, rather than fibres. At higher concentrations, above the critical entanglement limit for the polymer, the polymer chains are stretched and orientated whilst the solvent rapidly evaporates, delivering high aspect ratio fibres. The resulting mesh of overlapping fibres frequently has useful properties such as high surface area and porosity, which has led to their investigation for a range of applications including filtration membranes and tissue scaffolds. One of the major challenges in the development of electrospinning as a manufacturing technology is the use of organic solvents. Typically, fibres are spun from relatively dilute solutions containing 95% solvent. It is clear that systems which use water as a solvent offer many advantages in terms of safety, cost and sustainability. In this work we optimise the conditions for effectively preparing nano/micro fibres of polyethylene oxide from aqueous solutions. We contrast the fibres produced with those prepared using volatile organic solvents.

© 2017 Published by Elsevier B.V. This is an open access article under the CC BY-NC-ND license (<http://creativecommons.org/licenses/by-nc-nd/4.0/>).

Peer-review under responsibility of the scientific committee of the International Conference on Sustainable and Intelligent Manufacturing

\* Corresponding author. Tel.: +351-244-569-441  
E-mail address: [geoffrey.mitchell@ipleiria.pt](mailto:geoffrey.mitchell@ipleiria.pt)

*Keywords:* Electrospinning; Sustainability; nano/micro fibres.

---

## 1. Introduction

Electrospinning is a technique that has gained significant attention in the past decades due to the ease of production of microscale to nanoscale sized polymer fibres along with the potential applications that these fibres can offer. The technique is relatively simple requiring a polymer and a suitable solvent (that is one possessing a sufficiently high dielectric constant), a high voltage source, a grounded target electrode and a syringe pump to provide a constant flow of material [1]. The polymer is dissolved in the solvent and then loaded into a syringe with a needle attached. The syringe containing the solution is then placed into the syringe pump with the high voltage probe attached at the needle. As the voltage is applied the droplet of polymer solution at the needle tip will deform above a threshold voltage into a conical shape, often referred to as a Taylor cone [2], from which a jet will be extruded towards a target at a lower potential. Typically a grounded flat electrode is used which will collect material in a randomly orientated non-woven mat, alternatively if a common alignment of the fibres is desired a grounded rotating collector is used [1,3,4]. On moving from the needle tip to the collector the polymer jet will experience what is referred to as a bending instability, which is a whipping back and forth of the polymer jet [5]. This tends to result in stretching of the material as it transits towards the collector, thinning the jet diameter significantly, simultaneously solvent will be forced off the jet and solidification occurs on route. The fibres produced with this technique exhibit diameters of the order of several micrometres down to ten's of nanometres, with a degree of controllability offered through selecting parameters such as the polymer molecular weight, solution concentration and the solvent used, which will all influence the solution viscosity [6,7]. Other parameters such as the applied voltage and needle tip to collector distance will also have an impact, but to a lesser extent than control of the solution parameters [6]. The control over solution parameters is key in the development of solutions with sufficient chain entanglements to develop smooth continuous fibres. At low concentrations solutions tend to produce discrete droplets, with increasing concentrations of polymer leading to the development of beaded fibres and finally smooth, continuous fibres above a critical entanglement limit [6-10].

The properties of these fibres offer many diverse potential applications such as electronics [11], textiles [12], filtration [13], catalysts [14], oil recovery [15], reinforcement agents in composite materials [16], and biomedical applications such as drug delivery [17], wound dressings [18] or tissue engineering scaffolds [19]. The wide variety of possible applications can make them particularly attractive to industry, however there are notable drawbacks. Large scale production of materials requires scaling up of equipment to achieve significant enough throughput for industrial needs. There are now industrial scale production methods currently available such as the Elmarco Nanospider which offer significantly higher throughput than lab scale production methods [20]. Another drawback to the technique relates to the issues of sustainability. In many cases organic solvents are used to dissolve the polymer, the volatilization of these during the spinning process may exacerbate the hazards associated with the use of such solvents including flammability toxicity and in some cases even carcinogenicity; in addition the process is wasteful. As a consequence of this large scale use of such solvents in industry can be unattractive. There are alternative options such as melt electrospinning where no solvent is required; however the majority of research articles report on fibre diameters in the micrometre range with few exceptions [1]. The best and most sustainable route aspect is the use of a water soluble polymers in the electrospinning process.

### 1.1. Water soluble polymers

Of the range of water soluble polymer that are available, some of the most common ones that have been used in the electrospinning process are polyvinylpyrrolidone (PVP) [21,23], polyvinyl alcohol (PVA) [24,25], polyacrylic acid (PAA) [26,27], Gelatine [28] and polyethylene oxide (PEO). For this particular study we have selected to use polyethylene oxide. PEO is a low toxicity material currently used in a variety of applications, for example, for pharmaceutical products. The material is often available in a variety of molecular weights, ranging from 20,000 Da up to several million Da [molecular weights that are lower than 20,000 Da are often referred to as polyethylene glycol (PEG)]. In terms of electrospinning a sufficiently long chain length is required for entanglements to form in

solution to facilitate the formation of fibres rather than droplets. Thus the wide variety of molecular weights available for PEO can give many options, the real benefit of the material however is its water solubility providing a more sustainable less hazardous route to nanofibre production. Furthermore, the high dielectric constant of water makes it particularly suited to the electrospinning process often aiding in producing fibres with a reduced diameter [29]. Table 1 shows a list of commonly used solvents in the electrospinning process that can be used for the dissolution of PEO or have been used in the electrospinning of PEO on previous occasions, either on its own or as a co-solvent.

Table 1: List of solvents that have been previously used in the electrospinning of PEO with a few properties listed. [30]

Solvent	Formula	Boiling point (°C)	Dielectric constant	Surface Tension (mNm <sup>-1</sup> )	Dipole Moment (D)	Hazards <sup>a</sup>	1.1.1. PEL (TWA 8 hours) <sup>b</sup>
Acetic acid [31,32]	CH <sub>3</sub> COOH	118	6.2	27.8	1.74	Corr	10 ppm (25 mg/m <sup>3</sup> ) [33,34]
Chloroform [29,35]	CHCl <sub>3</sub>	61	4.8	27.14	1.04	K/P. Carc	50 ppm (240 mg/m <sup>3</sup> ) [36]
Dichloromethane [37]	CH <sub>2</sub> Cl <sub>2</sub>	40	8.9	26.52	1.6	F, P. Carc, Tox	25 ppm (87 mg/m <sup>3</sup> ) [38,39]
1,2-Dichloroethane	C <sub>2</sub> H <sub>4</sub> Cl <sub>2</sub>	84	10.4	38.75	1.80	Carc	50 ppm (200 mg/m <sup>3</sup> ) [40]
Dimethylformamide [29]	C <sub>3</sub> H <sub>7</sub> NO	153	38	37.1	3.82	F, Ter	10 ppm (30 mg/m <sup>3</sup> ) [41,42]
Ethanol [29,43-45]	C <sub>2</sub> H <sub>6</sub> O	79	30	22.75	1.69	F	1,000 ppm (1,900 mg/m <sup>3</sup> ) [46,47]
Isopropanol [48]	CH <sub>2</sub> OH	82	18	21.7	1.66	F, Tox	400 ppm (980 mg/m <sup>3</sup> ) [49]
Water [29,45,50]	H <sub>2</sub> O	100	80.1	73.05	1.85		

<sup>a</sup> (Corr - corrosive, Carc - Carcinogen, K/P. Carc - Known or possible carcinogen, F - flammable Ter - Teratogen and Tox - Toxic). (PEL - Permissible exposure limit, TWA - Time weighted average).

From Table 1 the various dangers and permissible exposure limits over an 8 hour period can be seen for several organic solvents, further emphasising the benefits of the use of a water soluble material. In addition to the benefits of having a water soluble material for use in an industrial setting, there is also the added benefit for obtaining approved use of materials in the biomedical sector, where materials processed from hazardous chemicals are less likely to be approved for use. PEO is currently used in pharmacy for oral drug delivery due to its biocompatibility [51].

Previous studies of electrospinning of PEO have shown that it readily produces fibres on length scales from nanoscale to microscale from organic solvents as well as water (Several references provided in Table 1). Not only has it proved to be a useful material for electrospinning on its own, but it has proven to serve as a binding agent to aid in the electrospinning of biomaterials that are not readily spinnable, such as silk [52], lignin [53], alginate [54,55], whey protein isolate [56] and eggshell proteins [57].

In this article we describe the optimization of conditions for electrospinning PEO from water by examining the impact that changes in polymer concentration has on the fibre morphology, and contrast this to PEO fibres prepared from two organic solvents, namely dichloromethane (DCM) and acetic acid (AcOH). We also examine any potential impact on the polymer morphology due to the spinning process as well as the effect that any potential change in solvent may incur. These are important considerations to take into account as the morphology developed can impact on the applicability of such fibres for their intended uses.

## 2. Materials and Methods

### 2.1. Polymers and Solvents

Polyethylene oxide with a molecular weight ( $M_v$ ) of 200,000 Da, was purchased from Sigma-Aldrich. The solvents used were deionised water (DIW), dichloromethane (DCM) (Sigma-Aldrich) and acetic acid (AcOH) (Sigma-Aldrich).

### 2.2. Solution Preparation

Solutions were prepared by measuring the appropriate quantity of polymer into a sample bottle, then adding the desired volume of solvent to produce specific concentrations. The material was left up 2 days to allow it sufficient time to dissolve. After dissolution the solution was placed on a vortex mixer for several minutes to ensure the solutions were homogeneous. Here the solutions percentages are defined as the quantity of polymer weight in 10 mL, for example 10% is 1 gram of polymer in 10 mL of solvent and 20% is 2 grams in 10 mL.

### 2.3. Electrospinning

Electrospinning was performed using a Glassman's high voltage power supply capable of delivering 0 – 30 kV with respect to ground. Solutions were loaded into a 5 ml glass syringe fitted with a 22 gauge Luer lock metal needle (0.413 mm internal diameter) of length 50 mm to which the high voltage supply was attached. The syringe containing the polymer solution was loaded onto a Razel scientific syringe pump and a solution flow rate of 1.78 ml/hr was used to supply the needle tip with a constant supply of fresh material. The distance between the rotating collector and needle tip was 15 cm and the applied voltage of 10 kV was used. Samples were collected onto a rotating collector at varying surface tangential velocities between  $0.7 \text{ ms}^{-1}$  to  $4.7 \text{ ms}^{-1}$ .

### 2.4. Microscopic analysis

Scanning electron microscopy (SEM) was performed at 20kV using a SEM 360 (Cambridge Instruments). Samples of foil coated with the fibres were sectioned from the electrospinning collector plate and mounted onto small SEM aluminium stubs via sticky conducting carbon tabs. Samples were then sputter coated with a thin layer of gold prior to examination in the SEM. Image-analysis was conducted with the software packages, Scandium and ImageJ to determine the diameters/sizes and orientations of the various fibrous/non-fibrous products. An ImageJ macro, OrientationJ was used to aid in measurements of the fibre orientations [58, 59].

### 2.5. Small Angle and Wide Angle X-ray Scattering

Small angle x-ray scattering (SAXS) and wide angle x-ray scattering (WAXS) experiments were performed on the Bruker AXS Nanostar in the University of Reading Chemical Analysis Facility, UK. The equipment has a compact 3 pin hole collimation and a beam size less than 1 mm (0.4 mm to 0.8 mm). SAXS and WAXS data were collected simultaneously with the small angle data collected on to a 2D 2048 x 2048 pixel frame detector approximately 66 cm distance from the sample. 2D WAXS patterns were collected onto an image plate placed approximately 10 cm from the sample position. A hole in the centre of the WAXS image plate allows for the simultaneous collection of SAXS data. Data was collected from  $Q = 0.015 \text{ \AA}^{-1} - 5 \text{ \AA}^{-1}$  where  $Q = 4\pi\sin\theta/\lambda$ ,  $\lambda$  is the wavelength and  $2\theta$  is the scattering angle. A wavelength of  $1.54 \text{ \AA}$  was employed. Sample data was collected for 15 – 30 minutes. For calibration of the SAXS data a silver behenate standard was used and a corundum standard was used for WAXS calibrations to obtain the sample to detector distance using the known  $Q$  values of the diffraction rings of these standards. Calibrations and data reductions to 1D plots were performed in imageJ using the macro YAX 2.1 [58, 60].



## Results and Discussion

### 3.1. Scanning Electron Microscopy

Examination of the fibre morphology was conducted using SEM with samples collected at varying solvent, polymer concentrations and surface tangential speeds of the rotating collector. The SEM micrographs presented in Fig. 1 are for the samples collected at a surface tangential velocity of  $2.7 \text{ ms}^{-1}$  whilst the polymer concentration and solvent used in fibre preparation were varied. From the micrographs it can be observed that the samples prepared from DIW (Fig. 1a - 1c) reveal the structural development from beaded material at 10% (Fig. 1a), to beaded fibres at 15% (Fig. 1b) and finally to that of aligned arrays of smooth, continuous electrospun fibres at 20% (Fig. 1c). Measurements of the fibres spun from DIW with a polymer concentration of 15% possess an average fibre diameter of  $(169 \pm 72) \text{ nm}$ , whilst at 20% the fibre diameter has increases to an average of  $(186 \pm 50) \text{ nm}$ . The transition from the beaded form to smooth continuous fibres has been associated with a required chain entanglement necessary for their production [8-10].

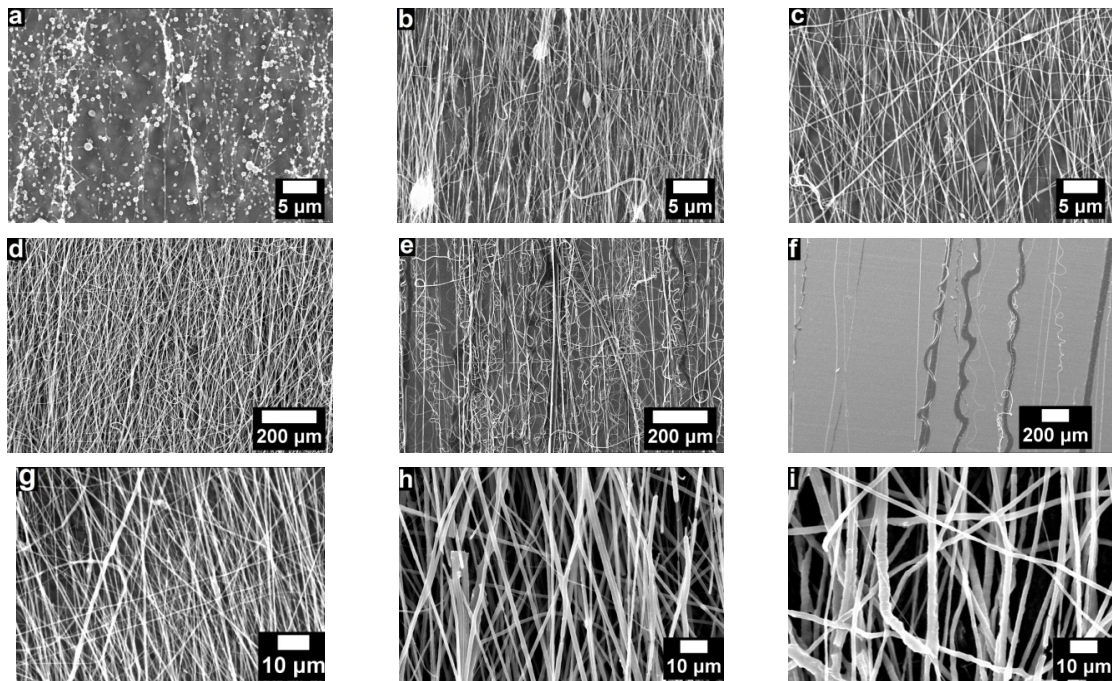


Fig. 1. Electrospun fibres prepared at increasing solution concentration (from left to right) and different solvents. a - c) samples prepared from DIW at 10%, 15% and 20% d - f) samples prepared from DCM at 10%, 15% and 20% g - i) samples prepared from AcOH at 10%, 15% and 20%

Samples that were prepared from DCM (Fig. 1d - 1f) show significantly larger diameters than those spun from DIW, with diameters measuring in the micrometre range ( $1.8 \pm 0.7 \mu\text{m}$ ) at 10% (Fig. 1d) and ( $3.3 \pm 2.7 \mu\text{m}$ ) at 15% (Fig. 1e). The 15% samples also exhibits some twisting/curling of the deposited fibres and a larger diameter distribution than those spun at 10%. For the samples prepared from 20% in DCM a severely reduced fibre yield was observed with only a few very large and several smaller fibres produced (Fig. 1f), with the average fibre diameter measured at  $17.8 \mu\text{m}$ . This type of behaviour is typical for high concentration solutions where there may be difficulties in pumping the solution through the syringe, insufficient force to overcome the surface tension effects of the polymer droplet, or the droplet at the needle tip rapidly dries up stopping the spinning process [61]. For the material that is successfully pulled from the droplet at the needle tip, it appears that less stretching occurs resulting in the larger fibre diameters that are observed. This may be attributed to a combination of the droplet drying out

along with the high viscosity of the material preventing sufficient whipping of the material. The spinnability of the solutions were significantly improved at polymer concentrations less than 20%, with 10% showing generally smaller diameter fibres and a narrower fibre diameter distribution.

The samples that were prepared from AcOH (Fig. 1g - 1i) exhibited a smaller average fibre diameter than those produced from DCM, but the average fibre diameters still remained larger than those prepared from DIW for similar concentrations. Fibres spun at 10% were  $(480 \pm 212)$  nm (Fig. 1g). At 15% the fibre diameters measured in the micrometre range  $(1.2 \pm 0.3)$   $\mu\text{m}$  (Fig. 1h) and at 20%  $(1.9 \pm 0.6)$   $\mu\text{m}$  (Fig. 1i). The samples prepared from AcOH in this study all exhibited smooth, continuous features, with no signs of larger fibres produced as was observed with DCM, and no beading at the lower concentrations as observed when fibres were spun from DIW. Fig. 2a shows a plot of the how the concentration and solvent influences the average fibre diameter for samples collected at a surface tangential velocity of  $2.7 \text{ ms}^{-1}$ . The results of Fig. 2a reiterate the information stated above that the samples prepared from DCM show the largest diameters, those from AcOH are smaller, but remain larger than those samples prepared from DIW.

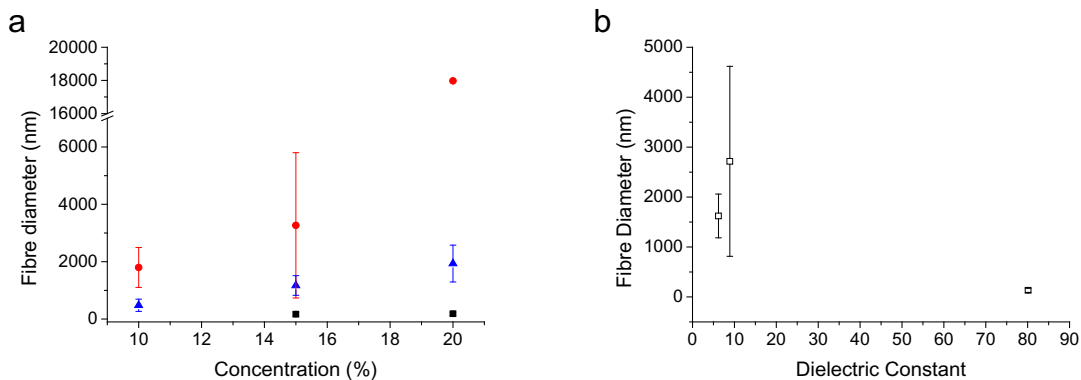


Fig 2: a) Plot of average fibre diameter as a function of solution concentration that the samples were prepared from for samples collected on a rotating collector with surface tangential velocity at  $2.7 \text{ ms}^{-1}$ . Symbols represent samples prepared from DIW (■), DCM (●) and AcOH (▲). b) Plot of average fibre diameter vs. solvent dielectric constant for samples prepared from 15% PEO in solvent, collected on the rotating collector at a surface tangential velocity of  $0.7 \text{ ms}^{-1}$

Figure 2b shows a plot of the dielectric constant of the solvent vs. the average fibre diameter. The results suggest that the higher dielectric constant is beneficial to the spinning process, as was previously shown in work conducted by Son *et al.* [29]. Son *et al.* examined a series of different solvents from the study here and one observation that differs in this work relates to the fibres prepared from DCM. In this study fibres prepared from DCM exhibited a larger fibre diameter than those spun from AcOH, despite DCM having a slightly larger dielectric constant. This may be due to the boiling point of DCM being quite low ( $40^\circ\text{C}$ ) which results in a rapid evaporation of the solvent and significantly less stretching of the jet as compared to AcOH which is not as easily removed as DCM.

Examination of micrographs for fibres prepared from the same concentration solution, but increasing collector speed show an improvement in orientation from a nearly randomly orientated sample, to that of well aligned arrays of parallel fibres. Figure 3 shows an example of improving alignment with increasing collection speed for samples prepared from 20% PEO in DIW.



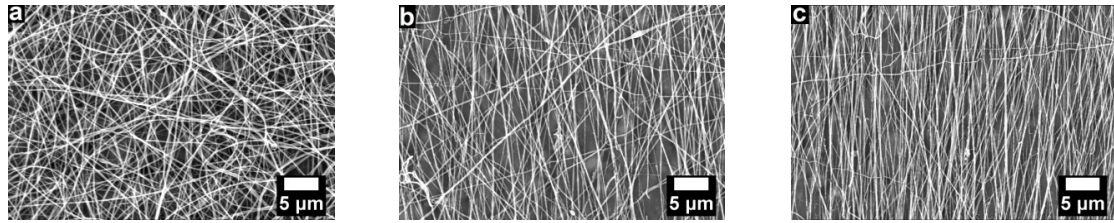


Fig 3: Electrospun fibres prepared from a 20% PEO in DIW collected at various surface tangential velocities of the rotating collector. Samples were collected at a)  $0.7 \text{ ms}^{-1}$  b)  $2.7 \text{ ms}^{-1}$  and c)  $4.7 \text{ ms}^{-1}$ .

Due to the erratic nature of the electrospinning process, which is attributed to charge repulsion along the elongating jet, the fibres are whipped back and forth in different directions and as a result, they are deposited in a random orientation against a flat collector surface [5,62]. The rotating collection system allows for the fibres to be aligned in an orientated fashion, with the level of orientation dependent on the rotational speeds of the collector used and the transition speed of the jet between the needle tip and collector surface. At surface tangential velocities that are lower than the jet transition velocity, the polymer jet is being extruded and deposited faster than the collectors rotation, resulting in no tension on the fibre and a more random orientation is observed. At higher surface tangential velocities, the surface of the collector is moving at a speed that is more comparable to the transit speed of the jet, allowing for a level of tension on the fibres and orientation to be developed. At higher speeds still, the level of tension is capable of stretching the polymer jet thereby deforming and thinning the fibres [63,64].

We can determine an orientation parameter,  $\langle P_2 \rangle_f$  calculated from  $(3(\cos^2\theta)-1)/2$  describing the level of orientation of the fibres. For fibres that are perfectly aligned vertically  $\langle P_2 \rangle_f = 1$  and for a randomly orientated sample  $\langle P_2 \rangle_f = 0$ . For samples that are aligned horizontally  $\langle P_2 \rangle_f = -0.5$ . Using the SEM micrographs, we can determine  $\langle P_2 \rangle_f$  values for the sample by measuring the variation in the angle from that of the direction of rotation for the collector (defined here as vertical on page). The fibre diameters (Fig. 4a) and orientation parameter (Fig. 4b) as a function of the surface tangential velocity of the rotating collector is shown in Fig. 4 for the various samples spun.

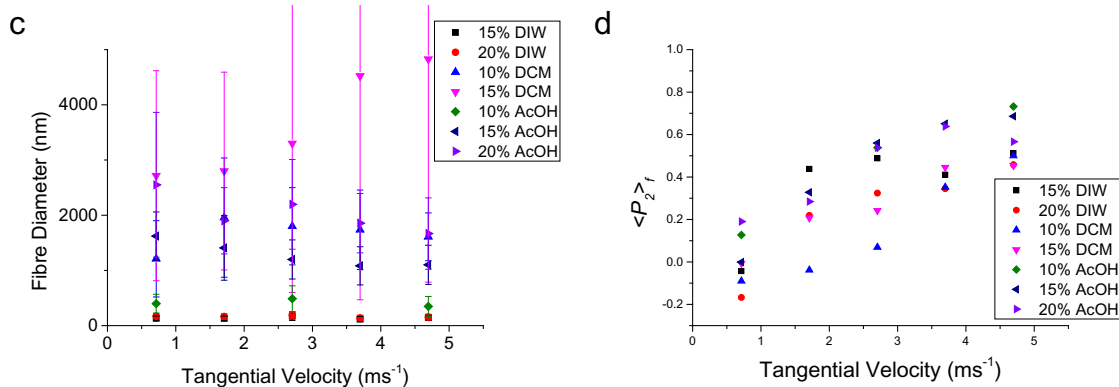


Fig 4: a) Average fibre diameter and b) Orientation parameter for the fibre axes as a function of rotating collector for PEO solutions spun from DIW, DCM and AcOH at concentrations of 10%, 15% and 20% for increasing surface tangential velocities of the rotating collector

Figure 4a corroborates the information stated earlier that the fibres prepared from DIW exhibit the smallest diameter, whilst those spun from DCM exhibited the largest diameters in this study. There is little impact on the observed fibre diameters as a function of collection speeds used in this study for the samples prepared from DIW and 10% PEO in DCM. The samples prepared from AcOH did display some changes in the fibre dimensions as the rotational velocity of the collector increased, with the fibre diameter decreasing from  $\sim 1.6 \mu\text{m}$  at  $0.7 \text{ ms}^{-1}$  to  $1.1 \mu\text{m}$

at  $4.7 \text{ ms}^{-1}$  for the 15% PEO solution. A similarly observable trend was apparent for samples prepared from the 20% PEO in AcOH solution where the decrease was more substantial, dropping from  $\sim 2.5 \text{ }\mu\text{m}$  at  $0.7 \text{ ms}^{-1}$  to  $1.7 \text{ }\mu\text{m}$  at  $4.7 \text{ ms}^{-1}$ . There was also a decrease in the standard deviation of the fibre diameter distribution with the increasing collection speed for both of these data sets, indicating a narrowing of the fibre diameter distribution. This would indicate that the samples may be experiencing a level of mechanical deformation imparted from the rotating collector, similar to observations previously made by Edwards *et al.* [64] and Mohan *et al.* [63]. Unusually the samples prepared at 15% PEO in DCM exhibited an increasing fibre diameter with increasing tangential velocity, the opposite of what would be expected. These observations may be the result of a combination of high viscosities reducing the spinnability and an impact on fibre formation from the increased airflow due to the higher rotating collector velocities, either disrupting fibre formation or causing a more rapid drying of the droplet at the needle tip. It was observed by eye that during the spinning of these samples, large droplets would form at the needle tip, apparently drying out before falling off and then droplets reformed; thus the samples collected at the higher velocities showed reduced fibre output as well as a larger average fibre diameters.

Figure 4b shows that there is a substantial improvement in the orientation of the alignment of the fibres with an increasing surface tangential velocity of the rotating collector. The data shows that at surface tangential velocities of  $0.7 \text{ ms}^{-1}$  the sample show little in terms of orientation with  $\langle P_2 \rangle_f$  values lying between  $-0.2$  to  $+0.2$ . At this surface tangential speed there is insufficient tension applied on the electrospinning jet to wind the fibres up as they are produced, hence the low level of orientation that is observed. The slightly negative  $\langle P_2 \rangle_f$  value for some of the prepared samples is an indication of some preferential deposition of the fibres along the length of the collector surface, possibly the result of electric field interactions. The samples that were prepared from DIW and DCM reach a  $\langle P_2 \rangle_f \sim 0.5$  at the higher surface tangential velocities. It is possible that higher orientations are achievable at greater tangential velocities than those used in this study. The data for 10%, 15% and 20% PEO in AcOH show alignment developing at relatively low tangential velocities of  $2.7 \text{ ms}^{-1}$  where  $\langle P_2 \rangle_f \sim 0.5$ . As stated previously, the development of the orientation is dependent on the rotational velocity of the collector being comparable to the jet transition speed. Development of orientation at low rotational velocities would indicate that the jet speed for the samples prepared from AcOH were relatively low. At higher velocities the collector surface may be moving faster than the jet and so the sample is being mechanically deformed, which would account for the decrease in average fibre diameter for the 15% and 20% PEO in AcOH solutions. The samples that exhibited the highest level of fibre orientation in this study were those prepared from AcOH, where  $\langle P_2 \rangle_f$  values range from  $0.63 - 0.73$ .

### 3.2. SAXS/WAXS Data

Selected samples were subjected to examination with SAXS/WAXS. These samples were all prepared from solution concentrations of 15% in DIW, DCM and AcOH, with the collector's surface tangential velocity at  $4.7 \text{ ms}^{-1}$ , the samples that exhibited the highest degree of fibre alignment. The scattering patterns,  $S(|Q|, \alpha)$  will exhibit uniaxial symmetry so we can describe the level of anisotropy in the samples by using the coefficients of a series of even ordered Legendre polynomials  $P_{2n}$ . In this case we restrict our attention to the second term,  $P_2$  which can be evaluated using

$$\langle P_2 \rangle_0 = \frac{\int_0^{\pi/2} S(|Q|, \alpha) P_2(\cos \alpha) \sin \alpha d\alpha}{\int_0^{\pi/2} S(|Q|, \alpha) \sin \alpha d\alpha} \quad (1)$$

Equivalent expressions apply for the 3 symmetry related quadrants of the scattering pattern. The level of preferred orientation of the crystals in the fibres  $\langle P_2 \rangle_c$  can be obtained using the methodology based on the Legendre Addition Theorem [64-66];  $\langle P_2 \rangle_c = \langle P_2 \rangle / \langle P_2 \rangle_f$  where  $\langle P_2 \rangle$  is the result of the crystalline orientation obtained from the experimental scattering pattern with respect to the collection direction and  $\langle P_2 \rangle_f$  is the orientation parameter of the fibre samples measured earlier (fig. 4b). 2D WAXS data shows a low level of orientation of the diffraction ring at  $Q = 1.36 \text{ \AA}^{-1}$  ([120] scattering plane) for which the  $\langle P_2 \rangle$  values for the samples were evaluated. To improve the

measure of anisotropy related to the orientation of the scattering pattern, the fibre samples that exhibited the highest alignment were chosen.

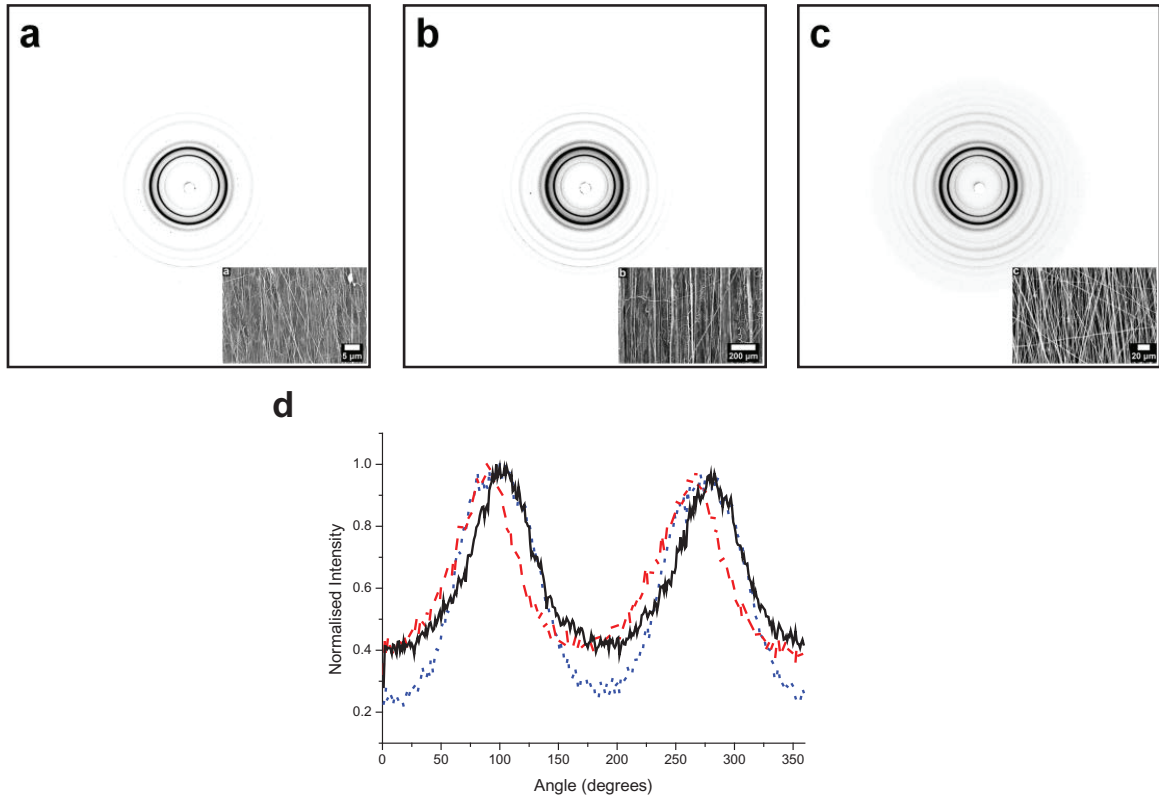


Figure 5: 2D WAXS data for fibres spun from 15% PEO in a) DIW, b) DCM and c) AcOH at  $4.7 \text{ ms}^{-1}$ . Insets are the SEM micrographs of the samples spun. d) 1D scattering intensity as a function of azimuthal angle for the diffraction ring at  $Q \sim 1.36 \text{ \AA}^{-1}$ . The solid black line represents the data for DIW, the red dashed line DCM and the blue dashed line AcOH.

Fig 5 a-c shows the obtained 2D WAXS patterns for the samples collected onto the rotating collector at a surface tangential velocity of  $4.7 \text{ ms}^{-1}$  for fibres prepared from 15% PEO in DIW (fig. 5a), DCM (fig. 5b) and AcOH (fig. 5c).  $\langle P_2 \rangle_c$  values of the diffraction ring at  $Q \sim 1.36 \text{ \AA}^{-1}$  were determined from the 2D patterns in fig. 5a-c by measuring  $\langle P_2 \rangle$  of the diffraction ring with background subtracted, then correcting for the fibre alignment. The values obtained for  $\langle P_2 \rangle$ ,  $\langle P_2 \rangle_f$  and  $\langle P_2 \rangle_c$  for these 3 samples are shown in table 2 below:

Table 2: Crystal  $\langle P_2 \rangle$ , fibre ( $\langle P_2 \rangle_f$ ) and corrected crystal orientation ( $\langle P_2 \rangle_c$ ) parameters for the samples prepared from 15% DIW, DCM and AcOH collected at a surface tangential velocity of  $4.7 \text{ ms}^{-1}$

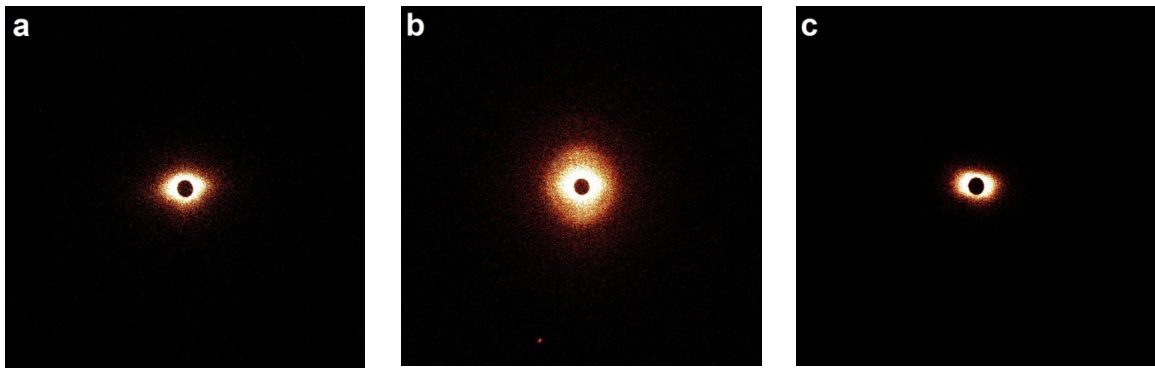
Solvent	$\langle P_2 \rangle$	$\langle P_2 \rangle_f$	$\langle P_2 \rangle_c$
DIW	0.198	0.513	0.386
DCM	0.218	0.454	0.480
AcOH	0.296	0.686	0.431

Fig. 5d provides a scaled version of the intensity variation with angle around the diffraction ring, offering a visual representation to the orientation measured in the scattering patterns. The scattering pattern of the sample spun from DIW revealed the lowest measured orientation whilst the sample spun from AcOH exhibited the highest level of orientation. The higher level of orientation measured in the scattering pattern for the fibres prepared from AcOH

may relate to the mechanical deformation imparted during the collection process. Similar observations have been previously made by Edwards *et al.* [64]. The samples prepared from DIW exhibited no noticeable changes in fibre diameter with increasing surface tangential velocity of the rotating collector, only an improvement in alignment, therefore we can assume that the level of anisotropy measured in the electrospun fibres is intrinsic to the spinning process itself. The fibres prepared from DCM displayed the inverse trend, with the fibres becoming larger at higher surface tangential velocities of the collector. Despite the larger average fibre diameter as compared to other samples, the orientation of the crystals is still comparable to that of those spun from DIW. This may be due to a deformation still being imparted from the collector onto the fibres despite their larger size.

The level of orientation measured in the scattering patterns would indicate that the impact between the different solvents does have an influence in the level of crystalline anisotropy developed within the fibres and hence may impact on certain applications the materials are designed for. This stems from the solvent used influencing the jet transition speed from needle tip to collector, which will impact on the stretching and thinning of the jet and the orientation developed within the sample. If the samples are being collected under tension to create aligned arrays of fibres, then mechanical deformation may result as seen here and in previous studies by Edwards *et al* [64]. For samples that would not be collected under tension, the induced crystalline orientation would be attributed to the electrospinning process itself, in which case samples spun from DIW exhibit a decent level of crystal orientation, where as the samples prepared from AcOH and DCM may require mechanical deformation to achieve similar levels.

2D SAXS data (fig. 6) reveals the preferential alignment of structures within the fibre samples. For the sample that was spun from DCM (fig. 6b) the scattering related to the lamellae is visible, with a higher scattering intensity present along the meridional plane. The increase of the intensity along the meridian indicates that the crystalline lamellae are stacked parallel along the length of the fibre axis. The 1D radial plot the scattering intensity vs. scattering vector for this data (fig. 6e) shows fall off in intensity at low to intermediate  $Q$  values varying as  $I(Q) \sim Q^{-3}$ , indicative of scattering from rough interfaces. The SEM micrographs show fairly smooth fibre surfaces, therefore it is possible that this scattering relates to the rough interface between the crystalline and amorphous phases, or possibly internal voiding within the fibres. After this fall off in intensity a small peak is observable at  $Q \sim 0.03 \text{ \AA}^{-1}$ , which arises from the crystalline lamellae (referred to as the long period,  $L_p$ ). For this sample  $L_p \sim 21 \text{ nm}$  ( $L_p = 2\pi/Q$ ).



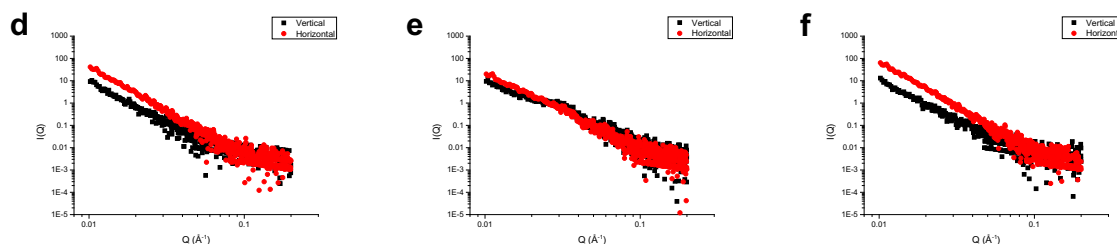


Fig. 6: 2D SAXS data and 1D SAXS of intensity vs. scattering vector for fibres spun from 15% PEO in a) DIW (1D plot of data in d) DCM (1D plot of data in e) and c) AcOH (1D plot of data in e) and collected onto the rotating collector at a surface tangential velocity of  $4.7 \text{ ms}^{-1}$ .

The samples spun from DIW and AcOH (fig. 6a and 6c) exhibit no scattering related to crystalline lamellae. The fibres prepared from DIW may be sufficiently small (ave. diameter  $(144 \pm 50) \text{ nm}$ ) that they do not exhibit lamellar stacks, with the crystalline structure possibly growing in a fibrillar form along the length of the fibre axis [67]. Despite the larger average fibre diameter of the fibres spun from AcOH (Ave. diameter  $(1102 \pm 355) \text{ nm}$ ), there appears to be a similar lack of scattering from crystalline lamellae. This may be due to fibres on the order of  $1 \mu\text{m}$  being sufficiently small enough that they do not develop the typical lamellar structure, or the mechanical deformation caused during the collection process was sufficient in inducing a similar fibrillar like crystal structure. The 1D plot of intensity vs. the scattering vector (fig. 6d and 6e), reveals that the scattered intensity falls off as  $I(Q) \sim Q^{-4}$  in the low  $Q$  to intermediate  $Q$  regimes for the samples prepared from DIW and AcOH. This power law fall off is indicative of samples that have sharp interfaces [68,69] and has been observed in fibres previously due to internal voiding in large microscale fibres [63,64,69]. The internally voided structures are usually associated with large microscale fibres that develop a skin during the spinning process and experience vapour induced phase separation [70,71]. However, the samples spun from DIW in this case are much smaller and are less likely to form an internal voided structure, whereas those spun from DCM and AcOH may develop such structures. The  $Q^{-4}$  scattering observed for the fibres spun from DIW is possibly due to a combination of the scattering from the small scale fibres themselves as well as elongated crystal structures, whereas the samples spun from AcOH are more likely a combination of internal voids and elongated crystals.

#### 4. Conclusions

Nanoscale fibres were produced using aqueous solutions of PEO and compared to those prepared from organic solvents, DCM and AcOH. Fibres spun from organic solvents tended to produced larger diameter fibres than those prepared from aqueous solutions. It was possible to adjust the spinning parameters so that arrays of nanoscale fibres were produced with a common macroscopic alignment through use of a rotating collector with surface tangential velocities comparable to the electrospinning jet transitions speed. The effects of the PEO concentration on electrospun fibre diameter was dependent on the solvent. The behavior of the aqueous solutions was markedly different to the organic solvents. PEO nanoscale fibres showed a preferred alignment of the crystals which formed with the c-axis parallel to the fibre axis; Higher levels of alignment was achieved with acetic acid as the solvent probably as a greater result of an enhanced level of deformation during the collection process.

#### Acknowledgements

The research leading to these results was partly funded by the European Union Seventh Framework Programme (FP7/2007-2013) under grant agreement number 263017, Project “NanoCelluComp”. GRM was funded by the Fundação para a Ciência e a Tecnologia (Portugal), through the Project reference UID/Multi/04,044/2013. SEM measurements were made at the EMLab, University of Reading, UK.

## References

- [1] Electrospinning: Principles, Practice and Possibilities (Ed: G. R. Mitchell), Royal Society of Chemistry, Cambridge 2015.
- [2] G. Taylor, Disintegration of Water Drops in an Electric Field, Proc. R. Soc. A, 280 (1964), 383-397
- [3] W.E. Teo and S Ramakrishna, A review on electrospinning design and nanofibre assemblies, Nanotechnology 17 (2006), R89–R106
- [4] Z.M. Huang, Y.Z. Zhang, M. Kotaki, S. Ramakrishna, A review on polymer nanofibers by electrospinning and their applications in nanocomposites, Compos. Sci. Technol. 63 (2003), 2223 - 2253
- [5] D.H. Reneker, A.L. Yarin H. Fong S. Koombhongse, Bending instability of electrically charged liquid jets of polymer solutions in electrospinning, Journal of Applied Physics, 87 (2000)
- [6] C. Wang, C-H Hsu, J-H Lin, Scaling Laws in Electrospinning of Polystyrene Solutions, Macromolecules, 2006, 39, 7662–7672
- [7] C Mit-uppatham, M Nithitanakul, P Supaphol, Ultrafine Electrospun Polyamide-6 Fibers: Effect of Solution Conditions on Morphology and Average Fiber Diameter, Macromol. Chem. Phys. 2004, 205, 2327–2338
- [8] M.G. McKee, G.L. Wilkes, R.H. Colby, T.E. Long, Correlations of Solution Rheology with Electrospun Fiber Formation of Linear and Branched Polyesters, Macromolecules, 2004, 37, 1760.
- [9] S.L. Shenoy., W.D. Bates, H.L. Frisch, G. Wnek. Role of chain entanglements on fiber formation during electrospinning of polymer solutions: good solvent, non-specific polymer–polymer interaction limit, E Polymer, 2005, 46, 3372–3384.
- [10] G. Eda, S Shivkumar, Bead-to-Fiber Transition in Electrospun Polystyrene, J. Appl. Poly. Sci., 106 (2007) 475–487
- [11] A. Luzio, E.V. Canesi, C. Bertarelli, M. Caironi, Electrospun Polymer Fibers for Electronic Applications, Materials, 7 (2014) 906-947
- [12] S. Lee S.K. Obendorf, Use of Electrospun Nanofiber Web for Protective Textile Materials as Barriers to Liquid Penetration, Textile Research Journal, 77 (2007) 696–702
- [13] R.S. Barhate, S. Ramakrishna, Nanofibrous filtering media: Filtration problems and solutions from tiny materials, J. Membrane Sci. 296 (2007), 296
- [14] S. Wen, M. Liang, R. Zou, Z. Wang, D. Yue L. Liu, Electrospinning of palladium/silica nanofibers for catalyst applications, RSC Adv., 5 (2015), 41513 - 41519
- [15] X. Wang, J. Yu, G. Sun, B. Ding, Electrospun nanofibrous materials: a versatile medium for effective oil/water separation, Materials Today 19 (2016) 403 - 414
- [16] Liao H, Wu Y, Wu M, Zhan X, Liu H, Aligned electrospun cellulose fibers reinforced epoxy resin composite films with high visible light transmittance. Cellulose 19 (2012) 111–119
- [17] C.Wang, K.-W. Yan, Y.-D. Lin and P. C. H. Hsieh, Biodegradable Core/Shell Fibers by Coaxial Electrospinning: Processing, Fiber Characterization, and Its Application in Sustained Drug Release, Macromolecules, 43 (2010) 6389 - 6397
- [18] M. Sadri, S. Arab-Sorkhi, H. Vatani A. Bagheri-Pebdeni, New wound dressing polymeric nanofiber containing green tea extract prepared by electrospinning method, Fibers and Polymers, 16 (2015) 1742–1750
- [19] E.J. Chong, T.T Phan, I.J. Lim, Y.Z. Zhang, B.H. Bay, S. Ramakrishna, C.T. Lim, Evaluation of electrospun PCL/gelatin nanofibrous scaffold for wound healing and layered dermal reconstitution, Acta Biomaterialia, 3 (2007), 321 - 330.
- [20] D. Petras, M. Maly, J. Pozner, J. Trdlicka, M. Kovac, United States Patent Application 20100034914, Assignee: Elmarco, S. R. O (Liberec, CZ) 2010.
- [21] S. Chuangchote, T. Sagawa, S. Yoshikawa, Electrospinning of poly(vinyl pyrrolidone): Effects of solvents on electrospinnability for the fabrication of poly(*p*-phenylene vinylene) and TiO<sub>2</sub> nanofibers, Journal of applied polymer science, 114 (2009) 2777 - 2791
- [22] M. Miyauchi, T.J. Simmons, J. Miao, J.E. Gagner, Z.H. Shriver, U. Aich, J.S. Dordick, R.J. Linhard, Electrospun polyvinylpyrrolidone fibers with high concentrations of ferromagnetic and superparamagnetic nanoparticles, ACS applied materials & interfaces, 3 (2011) 1958 - 1964
- [23] A.Y. Mikheeva, I.L. Kaneva, T.Y. Morozovaa, V. N. Morozov, Water-soluble filters from ultra-thin polyvinylpyrrolidone nanofibers, Journal of Membrane Science, 448 (2013) 151 - 159
- [24] C. Zhang, X. Yuan, L. Wu, Y. Han, J. Sheng, Study on morphology of electrospun poly(vinyl alcohol) mats, European Polymer Journal, 41 (2005) 423 - 432
- [25] P. Supaphol, S. Chuangchote, On the electrospinning of poly(vinyl alcohol) nanofiber mats: A revisit, 108 (2008) 969 - 978
- [26] B. Kim, H. Park, S.H. Lee, W.M. Sigmund, Poly(acrylic acid) nanofibers by electrospinning, Materials Letters, 59 (2005) 829 - 832
- [27] S. Xiao, M. Shen, H. Ma, R. Guo, M. Zhu, S. Wang, X. Shi, Fabrication of Water-Stable Electrospun Polyacrylic Acid-Based Nanofibrous Mats for Removal of Copper (II) Ions in Aqueous Solution, 116 (2010)
- [28] D.E. Elliott, F.J. Davis, G.R. Mitchell, R.H. Olley, Structure development in electrospun fibres of gelatin, Journal of Physics: Conference Series, 183 (2009) 012021
- [29] W.K. Son, J.H. Youk, T.S. Lee, W.H. Park, The effects of solution properties and polyelectrolyte on electrospinning of ultrafine poly(ethylene oxide) fibers, Polymer 45 (2004) 2959–2966
- [30] Handbook of Chemistry and Physics, ed. W.M. Haynes, CRC Press, Boca Raton, 95th edn, 1991
- [31] M. Pakravana, M.C. Heuzeya, A. Ajjia, A fundamental study of chitosan/PEO electrospinning, Polymer 52 (2011) 4813-4824
- [32] B. Duan, C. Dong, X. Yuan, K. Yao, Electrospinning of chitosan solutions in acetic acid with poly(ethylene oxide), J. Biomater Sci Polym Ed. 15 (2004) 797-811.
- [33] Centre for Disease Control [CDC], (Retrieved on: 29/01/2017), Retrieved from: <https://www.cdc.gov/niosh/docs/81-123/pdfs/0002-rev.pdf>
- [34] Occupational Health and Safety [OSHA], (Retrieved on: 29/01/2017), Regulations (Standards-29 CFR), Retrieved from: [https://www.osha.gov/dts/chemicalsampling/data/CH\\_216400.html](https://www.osha.gov/dts/chemicalsampling/data/CH_216400.html)
- [35] R. Jaeger, M.M. Bergshoeff, C.M. Batlle, H. Schlinherr, G.J. Vancso, Electrospinning of ultra-thin polymer fibers, Macromol. Symp. 127 (1998), 141-150



- [36] Occupational Health and Safety [OSHA] (29/01/2017) Retrieved from: [https://www.osha.gov/dts/chemicalsampling/data/CH\\_227600.html](https://www.osha.gov/dts/chemicalsampling/data/CH_227600.html)
- [37] J.E. Oliveira, L.H.C. Mattoso, W.J. Orts, E.S. Medeiros, Structural and Morphological Characterization of Micro and Nanofibers Produced by Electrospinning and Solution Blow Spinning: A Comparative Study, *Advances in Materials Science and Engineering*, 2013 (2013), 409572
- [38] Occupational Health and Safety [OSHA], (Retrieved on: 29/01/2017), Regulations (Standards-29 CFR), Retrieved from: <https://www.osha.gov/Publications/osha3144.html>
- [39] Occupational Health and Safety [OSHA], (Retrieved on: 29/01/2017), Regulations (Standards-29 CFR), Retrieved from: [https://www.osha.gov/dts/chemicalsampling/data/CH\\_253450.html](https://www.osha.gov/dts/chemicalsampling/data/CH_253450.html)
- [40] Occupational Health and Safety [OSHA], (Retrieved on: 29/01/2017), Regulations (Standards-29 CFR), Retrieved from: [https://www.osha.gov/dts/chemicalsampling/data/CH\\_240397.html](https://www.osha.gov/dts/chemicalsampling/data/CH_240397.html)
- [41] Occupational Health and Safety [OSHA], (Retrieved on: 29/01/2017), Regulations (Standards-29 CFR), Retrieved from: [https://www.osha.gov/dts/chemicalsampling/data/CH\\_236200.html](https://www.osha.gov/dts/chemicalsampling/data/CH_236200.html)
- [42] Centre for Disease Control [CDC], (Retrieved on: 29/01/2017), Retrieved from: <https://www.cdc.gov/niosh/docs/90-105/>
- [43] H. Fong, I. Chun, D.H. Reneker, Beaded nanofibers formed during electrospinning, *14* (1999) 4585–4592
- [44] T. Uyar, J. Hacaloglu, F. Besenbacher, Electrospun polyethylene oxide (PEO) nanofibers containing cyclodextrin inclusion complex, *J. Nanosci Nanotechnol.* 11 (2011) 3949-3958.
- [45] S.A. Theron, E. Zussman, A.L. Yarin, Experimental investigation of the governing parameters in the electrospinning of polymer solutions, *Polymer* 45 (2004) 2017–2030
- [46] Occupational Health and Safety [OSHA], (Retrieved on: 29/01/2017), Regulations (Standards-29 CFR), Retrieved from: [https://www.osha.gov/dts/chemicalsampling/data/CH\\_239700.html](https://www.osha.gov/dts/chemicalsampling/data/CH_239700.html)
- [47] Centre for Disease Control [CDC], (Retrieved on: 29/01/2017), Retrieved from: <https://www.cdc.gov/niosh/npg/npgd0262.html>
- [48] P.P. Tsai, H. Schreuder-Gibson, P. Gibson, Different electrostatic methods for making electret filters, *J. Electrostatics.* 54 (2002) 331-341
- [49] Centre for Disease Control [CDC], (Retrieved on: 29/01/2017), Retrieved from: <https://www.cdc.gov/niosh/npg/npgd0359.html>
- [50] J.M. Deitzel, J.D. Kleinmeyer, J.K. Hirvonen, N.C. Beck Tan, Controlled deposition of electrospun poly(ethylene oxide) fibers, *Polymer*, 42 (2001) 8163-8170
- [51] F. Ignatious, L. Sun, C.P. Lee, J. Baldoni, Electrospun Nanofibers in Oral Drug Delivery, *Pharmaceutical Research*, 27 (2010) 576 - 588
- [52] H. J. Jin, J. Chen, V. Karageorgiou, G.H. Altman, D.L. Kaplan, Human bone marrow stromal cell responses on electrospun silk fibroin mats, *Biomaterials*, 25 (2004) 1039-1047
- [53] V. Poursorkhabi, A.K. Mohanty, M. Misra, Electrospinning of Aqueous Lignin/Poly(ethylene oxide) Complexes, *J. Appl. Polym. Sci.* (2015) 41260
- [54] C.Hu, R. H. Gong, and F. L. Zhou, Electrospun Sodium Alginate/Polyethylene Oxide Fibers and Nanocoated Yarns, *International Journal of Polymer Science*, Volume 2015 (2015), Article ID 126041, 12 pages
- [55] Jian-Wei Lu, Yong-Liang Zhu, Zhao-Xia Guo, Ping Hu, Jian Yu. Electrospinning of sodium alginate with poly(ethylene oxide), *Polymer* 47 (2006) 8026-8031
- [56] A.C. Vega-Lugo, L.T. Lim, Effects of poly(ethylene oxide) and pH on the electrospinning of whey protein isolate, *Journal of Polymer Science B: Polymer Physics* 2012, 50, 1188-1197
- [57] J. Kang, M. Kotaki, S. Okubayashi, S. Sukigara, , Fabrication of electrospun eggshell membrane nanofibers by treatment with catechin, *Journal of Applied Polymer Science* 2009, 117, 2042-2049.
- [58] C.A. Schneider, W.S. Rasband, K.W. Eliceiri, NIH Image to ImageJ: 25 years of image analysis, *Nat Methods*, 9 (2012) 671-675.
- [59] R. Rezakhanliha, A. Agianniotis, J.T.C. Schrauwen, A. Griffla, D. Sage, C.V.C. Bouten, F.N. van de Vosse, M. Unser, N. Stergiopoulos, Experimental Investigation of Collagen Waviness and Orientation in the Arterial Adventitia Using Confocal Laser Scanning Microscopy, *Biomechanics and Modeling in Mechanobiology*, 11 (2012) 461-473.
- [60] S. L. Gras, A. M. Squires, *Methods Mol. Biol.*, 752 (2011), 147–163.
- [61] X. Zong, K. Kim, D. Fang, S. Ran, B.S. Hsiao, B. Chu, Structure and process relationship of electrospun bioabsorbable nanofiber membranes, *Polymer*, 43 (2002) 4403–4412
- [62] D.H. Reneker, A.L. Yarin, Electrospinning jets and polymer nanofibers, *Polymer*, 49 (2008) 2387 - 2425
- [63] S.D. Mohan, G.R. Mitchell, F.J. Davis, Chain extension in electrospun polystyrene fibres: a SANS study, *Soft Matter*, 7 (2011) 4397 - 4404
- [64] M. D. Edwards, G. R. Mitchell, S. D. Mohan and R. H. Olley, Development of orientation during electrospinning of fibres of poly( $\epsilon$ -caprolactone), *Eur. Polym. J.*, 46 (2010), 1175–1183.
- [65] R. Lovell and G. R. Mitchell, Molecular orientation distribution derived from an arbitrary reflection, *Acta Crystallogr., Sect. A: Cryst. Phys., Diffraction, Theor. Gen. Crystallogr.*, 1981, 37, 135–137
- [66] G. R. Mitchell, S. Saengsuwan and S. Bualek-Limcharoen, Evaluation of preferred orientation in multi-component polymer systems using x-ray scattering procedures, *Prog. Colloid Polym. Sci.*, 130 (2005) 149–158
- [67] M. Gazzano, C. Gualandi, A. Zucchelli, T. Sui, A.M. Korsunsky, C. Reinhard, M.L. Focarete, Structure-morphology correlation in electrospun fibers of semicrystalline polymers by simultaneous synchrotron SAXS-WAXD, *Polymer*, 63 (2015) 154-163
- [68] R.A. Pethrick, J.V. Dawkins, 1999 *Modern Techniques for Polymer Characterisation* (John Wiley)
- [69] S.D. Mohan, F.J. Davis, R.H. Olley, G.R. Mitchell, Modelling Small Angle Neutron Scattering Data from Electrospun Fibres, *Journal of Physics: Conference Series* 247 (2010) 012042
- [70] W. Liu, C. Huang, X. Jin, Tailoring the grooved texture of electrospun polystyrene nanofibers by controlling the solvent system and relative humidity, *Nanoscale Research Letters*, 9 (2014), 350
- [71] M. M. Demir, Investigation on glassy skin formation of porous polystyrene fibers electrospun from DMF, *eXPRESS Polymer Letters*, 4 (2010) 2–8